

PCCP

Accepted Manuscript



This is an *Accepted Manuscript*, which has been through the Royal Society of Chemistry peer review process and has been accepted for publication.

Accepted Manuscripts are published online shortly after acceptance, before technical editing, formatting and proof reading. Using this free service, authors can make their results available to the community, in citable form, before we publish the edited article. We will replace this *Accepted Manuscript* with the edited and formatted *Advance Article* as soon as it is available.

You can find more information about *Accepted Manuscripts* in the [Information for Authors](#).

Please note that technical editing may introduce minor changes to the text and/or graphics, which may alter content. The journal's standard [Terms & Conditions](#) and the [Ethical guidelines](#) still apply. In no event shall the Royal Society of Chemistry be held responsible for any errors or omissions in this *Accepted Manuscript* or any consequences arising from the use of any information it contains.

ARTICLE

Sodium-ion diffusion mechanisms in the low cost high voltage cathode material $\text{Na}_{2+\delta}\text{Fe}_{2-\delta/2}(\text{SO}_4)_3$

Cite this: DOI: 10.1039/x0xx00000x

L.L. Wong,^a H.M. Chen^a and S. Adams^aReceived 00th January 2014,
Accepted 00th January 2014

DOI: 10.1039/x0xx00000x

www.rsc.org/

Bond-valence site energy modelling, classical molecular dynamics and DFT simulations were employed to clarify Na^+ ion migration in monoclinic $\text{Na}_{2+\delta}\text{Fe}_{2-\delta/2}(\text{SO}_4)_3$, the recently reported first representative of a new promising class of alluaudite-type high voltage cathode material for sodium-ion batteries. Empirical potential parameters derived from our softBV bond valence parameter set reproduce experimental unit-cell parameters. Migration energy barrier calculations based on both these empirical and on ab initio approaches consistently show a strongly anisotropic and fairly fast Na^+ ion mobility along partially occupied Na(3) channels in the c-direction. Nominally fully occupied Na(1) sites are attached to these paths with a moderate activation energy as sources of mobile ions. At elevated temperatures separate parallel Na(2) channels contribute to the ionic conductivity. As such one-dimensional pathways are highly vulnerable to blocking by structural defects, the experimentally observed favourable rate performance can only be understood as a consequence of a cross-linking of the channels to a more robust higher-dimensional migration pathway network. Our static and dynamic bond valence pathway models for representative local structure models reveal that this cross-linking is achieved by the iron-deficiency of the compound: iron vacancies act as low-lying interstitial sites that can be reached from both types of channels with moderate activation energies. Structural relaxations around the vacancies however reduce the sodium mobility along the channels. An analogous dual effect of blocking migration along the channels and promoting perpendicular migration would result from $\text{Na}^+/\text{Fe}^{2+}$ antisite defects. Hence, further new alluaudite type transition metal sulphates can only be expected to yield a high rate performance, if their synthesis ensures the presence of a comparable transition metal sub-stoichiometry and/or a suitably tailored concentration of sodium/transition metal antisite defects.

1. Introduction

The renewed interest in Na-ion batteries due to the earth-abundance and low cost of sodium led to intensive exploration for a range of layered transition metal oxides as cathode materials.^{1,2} Despite the fact that the low price of active materials is a main driving factor for research into Na-based battery technologies, especially in the context of large scale batteries, most of this activity currently focuses on cathode materials containing relatively high cost transition metals such as Co and Ni that are also applied in Li-ion batteries. This is problematic not only because of the different reaction mechanism of the sodium analogues of the classical layered lithium transition metal oxides. The cost advantage of sodium over lithium will only translate into commercially viable large-scale Na-based batteries, if the concept of earth-abundant materials is consistently applied throughout their design.³ Hence, research on transition metal electrode materials for Na-based batteries has to concentrate on the most abundant transition metal Fe and

may explore metals with intermediate abundance such as Ti and Mn as alternatives. On the other hand, O3-type NaFeO_2 ^{4,5} and P2-type $\text{Na}_x[\text{Fe}_{0.5}\text{Mn}_{0.5}]\text{O}_2$ are known to suffer from limited reversible capacity and low operating potential despite the utilization of the $\text{Fe}^{4+}/\text{Fe}^{3+}$ redox couple. As for the analogous lithium compounds, the exploitation of the inductive effect of polyanion frameworks⁷ opened up the way to a range of Fe-based ternary or quaternary phosphates (NaFePO_4 ,⁸ $\text{Na}_2\text{FePO}_4\text{F}$,⁹ $\text{Na}_4\text{Fe}_3(\text{PO}_4)_2(\text{P}_2\text{O}_7)$ ¹⁰, $\text{Na}_2\text{FeP}_2\text{O}_7$ ¹¹) in which the $\text{Fe}^{3+}/\text{Fe}^{2+}$ redox couple yields about 3 V. Relying on the $\text{Fe}^{3+}/\text{Fe}^{2+}$ redox couple bears the added advantage that in these compounds the capacity of the one-electron reaction can be fully utilized without damaging the (kinetic) structural stability.

In order to further increase the cathode potential, phosphate units can be replaced by the more electronegative SO_4^{2-} units. While in contrast to analogous lithium compounds¹² the first studied sodium iron sulphates ($\text{NaFeSO}_4\text{F}\cdot x\text{H}_2\text{O}$, $x = 0, 2$) turned out to be electrochemically inactive,^{13,14} recently Barpanda et al.¹⁵ could synthesize so-called “ $\text{Na}_2\text{Fe}_2(\text{SO}_4)_3$ ” via

a low temperature solid state reaction and found that it combines an unusually high Fe redox potential of ~ 3.8 V versus Na (which corresponds to 4.1 V vs. Li/Li⁺) with excellent rate capability.

Unusually for sulphates, the structure of the compound described as Na₂Fe₂(SO₄)₃ adopts an alluaudite-type framework, where Fe₂O₁₀ groups formed by edge-sharing pairs of FeO₆ octahedra are bridged by corner-sharing sulphate groups to a three-dimensional framework with open tunnels that are occupied by three distinct types of Na⁺ ions (one fully occupied site Na(1) and two partially occupied sites). It may be noted that according to Mössbauer data reported in the same work, the two Fe²⁺ inside the Fe₂O₁₀ group should be distinct (which led the authors to a structure refinement in space group *P2₁/c*), while the atomic arrangement refined assuming this space group remains consistent with a higher-symmetry structure description in space group *C2/c*. At the stage of revision we became aware of a recent follow-up work by the same group describing both Na_{2.4}Fe_{1.8}(SO₄)₃ and its desodiated derivative Na_{0.89}Fe_{1.8}(SO₄)₃ as isostructural in space group *C2/c*.¹⁶ The relative orientation of the unit cells for both cell descriptions is visualized in Figure 1.

Refinements in both considered space groups yield a nearly identical substantial stoichiometry deviation that is only vaguely mentioned in the original main article,¹⁵ but specified as Na_{2+δ}Fe_{2-δ/2}(SO₄)₃ with $\delta \approx 0.25$ in its supplementary material. Since iron sulphate is the main impurity found in the sample, it may be assumed that this stoichiometry-deviation is an inherent property of the material at least for the chosen synthesis conditions and hence, in contrast to Barpanda et al.¹⁵, we chose to factor in this non-stoichiometry in our atomistic and ab initio simulations of this promising cathode material. As mentioned above, the same group more recently reported the preparation of non-stoichiometric Na_{2+δ}Fe_{2-δ/2}(SO₄)₃ with $\delta \approx 0.4$ and qualitatively discussed effects of the non-stoichiometry on applications of the chemically desodiated derivative Na_{0.89}Fe_{1.8}(SO₄)₃ as a lithium intercalation cathode.¹⁶ As already discussed by ref. [15], replacing the iron by Ti, Mn, Co, Ni, V or VO may lead to alternative cathodes/anodes and substitution by divalent main group cations might lead to compounds of interest as sodium (or lithium) solid electrolytes.

2. Computational Methods

2.1. Bond valence based forcefields for pathway analysis and molecular dynamics simulations

Migration pathways for the mobile Na⁺ are analysed both from literature crystal structure data and from series of snapshots of molecular dynamics (MD) simulations by our bond valence pathway method, as discussed elsewhere.^{17,18,19} This modelling of pathways for mobile alkali ions *A* as regions of low bond valence site energy $E_{BVSE}(A)$ has been demonstrated to be a simple and reliable way of identifying transport pathways in local structure models,^{19,20} provided that the local structure model captures the essential structural features. While bond

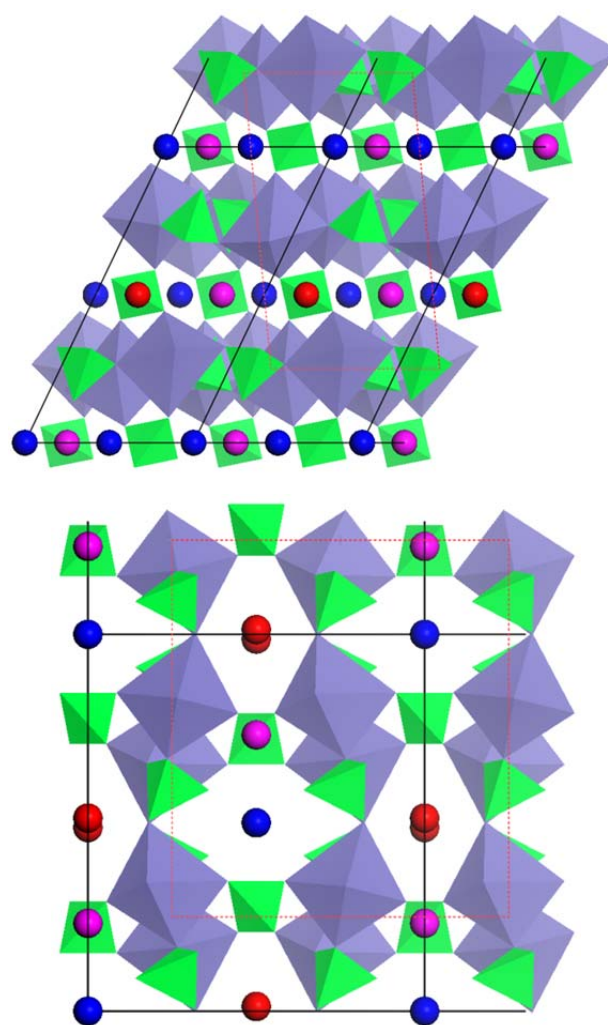


Fig. 1. Structure of Na_{2+δ}Fe_{2-δ/2}(SO₄)₃ viewed (a) along the *b*-direction, (b) along the *c*-direction. Na⁺ ions are shown as spheres (Na(1): magenta, Na(2): blue, Na(3): red), while SO₄ groups are displayed as light green tetrahedra and FeO₆ groups as dark blue octahedra. Black lines correspond to the unit cell when the structure is described in space group *C2/c* (as preferred in this work). Red broken lines mark the unit cell applicable for the lower symmetry description in *P2₁/c* (as suggested in ref. [15]).

valences $s_{A-X} = \exp[(R_{0,A-X} - R_{A-X}) / b_{A-X}]$ and hence the BV sum mismatch $|\Delta V|$ are often expressed in arbitrary “valence units”, they can, as elaborated by our group,^{21,22,23} be linked to an absolute energy scale by expressing the bond valence as a Morse-type interaction energy between cation *A* and anion *X*.

$$E_{BVSE}(A-X) = D \left[\sum_{i=1}^N \left(\left(\frac{s_{A-X}}{s_{\min,A-X}} \right)^2 - 2 \frac{s_{A-X}}{s_{\min,A-X}} \right) \right] + E_{repulsion} \quad (1)$$

The required bond valence parameters are taken from our *softBV* database as published in [22]. Migration pathways are analysed as regions of low $E_{BVSE}(\text{Na})$ in grids spanning the structure model with a resolution of ca. (0.1 Å)³. For the purpose of analysing $E_{BVSE}(\text{Na})$ landscapes Coulomb repulsions are considered only between mobile and immobile cations (here Na⁺-Fe²⁺, Na⁺-S⁶⁺), Coulomb attraction terms are generally

integrated into the Morse attraction term. Starting from an analysis of local minima and saddle points of $E_{BVSE}(\text{Na})$, the grid analysis utilizes a modified Dewar, Healy and Stewart (DHS)-type path finding algorithm to identify low energy paths connecting the local site energy minima.^{24,25}

The same empirical BV parameters b_{A-X} , $R_{0,A-X}$ used in this pathway analysis are also used as forcefield parameters for the generation of disordered local structure models by MD simulation. For the purpose of the MD simulations screened Coulomb repulsions $E_{\text{repulsion}}$ for all cation-cation and anion-anion pairs are included, while – as mentioned above – the repulsions among mobile ions are excluded for the purpose of pathway modelling. In both cases Coulomb repulsions are screened by an error function complement term

$$E_{\text{repulsion}}(A-B) = \frac{q_A \cdot q_B}{R(A-B)} \cdot \text{erfc}\left(\frac{R(A-B)}{f \cdot (r_A + r_B)}\right), \quad (2)$$

where r_A , r_B are the covalent radii of the respective cation (or anion) pair A , B and f is a factor (typically of the order $f \approx 0.75$, here $f = 0.742$) that is empirically linked to the electronegativity distribution in the respective crystal structure. Due to the favourable convergence of the chosen attraction and repulsion models a relatively short cut-off radius of 10 Å could be used enhancing computational efficiency. Both the Morse-type interactions and the Coulomb-repulsion terms are force-shifted to ensure zero energy gradients at the cut-off distance.

2.2. Molecular dynamics simulations

MD simulations have been conducted with the software GULP²⁶ as implemented in Materials Studio 6.0²⁷ using a Morse-type force field and the BV parameters of our *softBV* parameter set (cf. section 2.1) for a 918 atoms 2x2x3 supercell. The simulated cell composition $\text{Na}_{108}\text{Fe}_{90}(\text{SO}_4)_{144}$ corresponds to the fully discharged (i.e. fully sodiated) compound and factors in the experimentally observed amount of sodium excess and iron deficiency, since experimental reference structure data have been published for this composition only. It should be noted that for the MD simulations the orientation of the unit cell followed the $P2_1/c$ model, which yields a smaller deviation of the monoclinic angle from orthogonality so that the deviation of the supercell geometry from the computationally favourable isometric case is reduced. For each of the 15 temperatures in the range 300 – 800 K the bulk structure is initially equilibrated in NPT MD simulations (starting in the first simulation from the literature structure data, for subsequent temperatures from the last frame of the previous simulation). Then the relaxed volume is fixed and equilibration continued for 150 - 1000 ps followed by production runs of 400 ps (for 800 K) up to 60,000 ps for $T = 300$ K.

2.3. Density functional theory calculations

Density functional theory (DFT) calculations were performed with the Vienna *ab initio* simulation package VASP²⁸ using the projector augmented wave method²⁹ as implemented in the VASP code and assuming a PBE³⁰-type generalized gradient

approximation (GGA) exchange-correlation functional. A cutoff of 400 eV for the planewave expansion was used. In contrast to the approach chosen in ref. [15], here the Na-rich composition $\text{Na}_{2.25}\text{Fe}_{1.875}(\text{SO}_4)_3$ was modelled with a $1 \times 1 \times 2$ supercell leading to $\text{Na}_{18}\text{Fe}_{15}\text{S}_{24}\text{O}_{96}$ containing 153 atoms, so that empirical and *ab initio* calculations refer to the same composition. Additional geometry optimisations are conducted for various $\text{Na}_{18-x}\text{Fe}_{15}\text{S}_{24}\text{O}_{96}$ models, where one or two sodium atoms are removed from the structure model.

3. Results and Discussion

3.1. Bond valence site energy models of sodium migration pathways for the average crystal structure

Fig. 2 shows the sodium migration pathways derived from applying the bond valence site energy (BVSE) approach to the literature crystal structure data¹³ with site occupancy factors

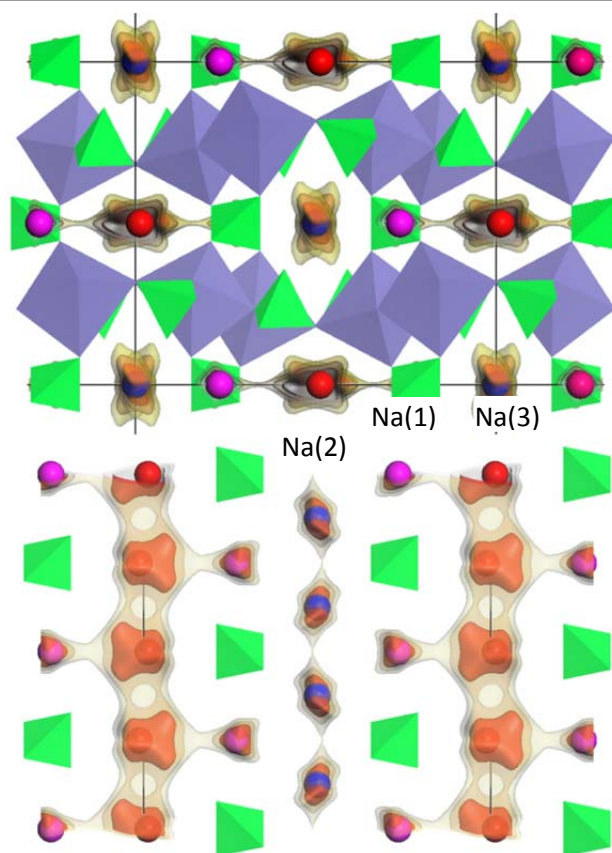


Fig. 2: (a) Bond valence site energy (BVSE) model of Na^+ -ion transport pathways superimposed on a structure model of $\text{Na}_{2.25}\text{Fe}_{1.875}(\text{SO}_4)_3$ viewed along the fast-ion conducting c direction. (b) Structure and bond valence model for a slice of the structure with $0.3 < x < 0.7$ projected onto the b - c plane showing the ribbon-type one-dimensional path along the partially occupied Na(3) sites in the c -direction, the attachment of Na(1) sites to this path as sources of mobile ions as well as the independent parallel one-dimensional path along the chain of Na(2) sites. In both graphs Na^+ ions are shown as spheres (Na(1): magenta, Na(2), blue, Na(3) red), while SO_4 groups are displayed as light green tetrahedra and FeO_6 groups as dark blue octahedra. The translucent isosurfaces of constant sodium BVSE correspond to equilibrium sites (red), the lowest energy ribbon-type pathway with $E_a \approx 0.3$ eV (orange). Only in the light yellow isosurface, corresponding to the highest energy of ca 0.8 eV, Na(1) sites are attached to the Na(3)-Na(3) pathway and the Na(2) ions form a separate one-dimensional path.

rounded to 1, 0.75, 0.5 and 0.9375 for Na(1), Na(2), Na(3) and Fe atoms, respectively. Thereby the underlying structure model is consistent with those used for the ab initio and MD computational studies in sections 3.3 and 3.4. It may be noted that the Na distribution itself does not affect the results of the static site energy models, while the Na-excess slightly affects simulation parameters (e.g. effective charges) and the Fe-deficiency directly affects the observed energy barriers. This simplified approach already yields a Na^+ ion migration pathway model that is essentially in line with the model derived from the literature ab initio analysis. As seen from Figures 2 and 3 the Na^+ ion migration will be essentially one-dimensional along the c-direction and follows the ribbon-type Na(3)-Na(3) pathway channel, due to the low activation energy of ca. 0.3 eV and favourable 50% occupancy of Na(3) sites ensuring a high success rate of attempted hops. The nominally fully occupied Na(1) ions can contribute additional mobile ions to the Na(3) channels with an activation energy that is estimated to 0.8 eV from this model. For the Na(2) ions (with a ca. 75% occupancy) the model predicts separate strictly one-dimensional paths along the c-direction with an activation energy of > 0.6 eV.

Semi-quantitatively the same migration paths were found in the literature ab initio study. The slight differences in quantitative migration barriers will partly be due to the different sodium content, as the DFT analysis resorted to the fully desodiated compound with a single probe Na^+ ion moved around to explore the energy landscape for the Na^+ ion, while our model refers to the experimental structure data for the fully sodiated compound. Thus in the BVSE analysis of $\text{Na}_{2.25}\text{Fe}_{1.875}(\text{SO}_4)_3$ seen in Figure 3 Na(1) sites, as to be expected, correspond to the lowest energy sites while a ca 0.2

eV higher site energy is found for the partially occupied Na(2) sites. In the literature DFT analysis for the hypothetical structure $\text{Na}_{0.125}\text{Fe}_2(\text{SO}_4)_3$ with (except for the probe Na^+) empty Na sites and full Fe site occupancy, the Na(2) site appears to have a slightly lower site energy. Similarly, the energy level of the Na(3) sites is raised in the desodiated compound, while the energy barrier between the Na(3) sites is hardly affected. Overall this pathway model suggesting one-dimensional pathways (with a high activation energy of nearly 1.4 eV to connect neighbouring Na paths to a dimensional network in the b-c plane) seems to be inconsistent with the observed favourable electrochemical performance for particle sizes of 100-200 μm synthesized by a low temperature non-equilibrium reaction path. Under such synthesis conditions it is unlikely that defect free one-dimensional channels spanning the entire crystallite will exist and thus the material will be highly vulnerable to blocking of the ion-conducting channels by defects, which should seriously reduce the rate capability of the material. On the other hand, Fe-deficiency may open up additional pathways cross-linking the fast-ion conducting channels to higher-dimensional pathway networks with moderate activation energy.^{18,23}

3.2. Sodium migration pathways for a representative local structure model

In order to explore the role of deviations of representative local structures from the average structure, we calculated Na-ion migration pathways for a local structure model derived from a $1 \times 1 \times 2$ superstructure of the experimental average structure by keeping the Na(1) site fully occupied, while randomly occupying 6 out of 8 Na(2) sites, 4 out of 8 Na(3) sites and 15

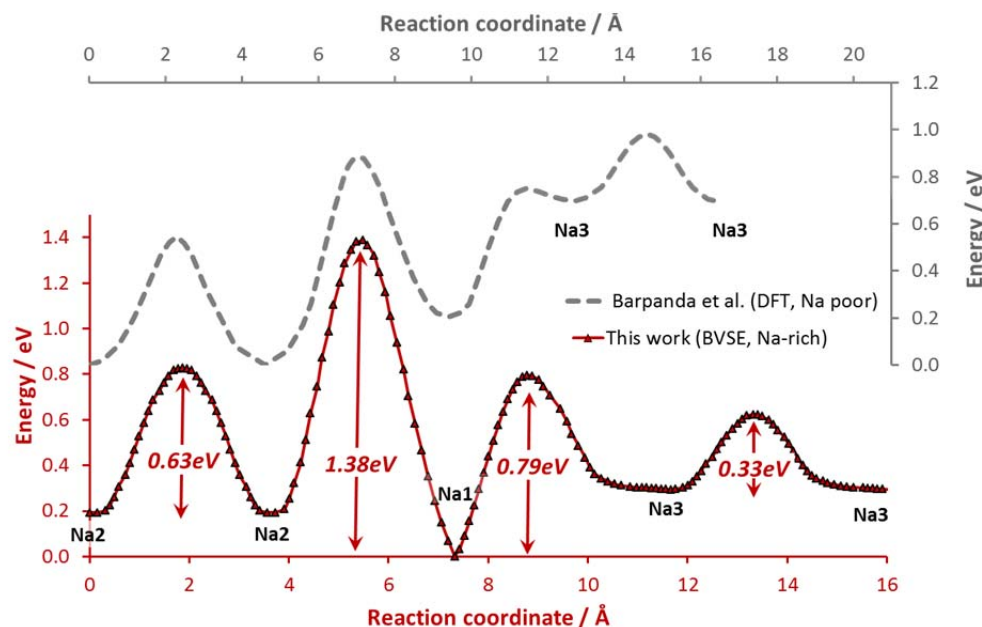


Fig. 3: Migration barriers for Na-ion diffusion in $\text{Na}_{2.25}\text{Fe}_{1.875}(\text{SO}_4)_3$ as derived from the bond valence site energy model for the experimental crystal structure data using a DHS-like path finding algorithm²⁴. The displayed values refer (from left to right) to migrations along the c axis for the Na(2) sites, the barrier separating Na(2) and Na(1) sites, the local path along the b direction connecting Na(1) to the chain of Na(3) sites, and to the lowest migration barrier for migration among Na(3) sites along the c axis. The bottom and left-hand side axes refer to these bond-valence based data. For comparison the DFT-derived migration barriers redrawn from [15] for a desodiated composition $\text{Na}_{0.125}\text{Fe}_2(\text{SO}_4)_3$ are shown in grey. The top and right-hand side axes refer to these DFT data.

ARTICLE

out of 16 Fe sites. The resulting structure was relaxed by constant volume geometry optimisation with the same bond-valence based forcefield that was also used for the MD simulations. Na^+ ion migration pathways in the resulting local structure model were analysed by the BVSE method sketched above. As shown in Figure 4 vacant Fe^{2+} sites act as low-lying

interstitial sites for Na^+ and link $\text{Na}(2)$ to $\text{Na}(3)$ sites with an activation energy barrier of 0.75 eV. Moreover, the relaxations in accordance to the local structure also lead to a significant variability of the energy barriers for the motion along the channels. Especially for the $\text{Na}(3)$ - $\text{Na}(3)$ chain at $y = 0.5$ the barrier near the vacant Fe site is increased substantially by the structural relaxation, here to 0.87 eV, more than three times higher than the 0.28(7) eV for other $\text{Na}(3)$ - $\text{Na}(3)$ in the same local structure model (cf. Figure 5). Thus, the $\text{Na}(3)$ - $\text{V}_{\text{Fe}^{2+}}$ - $\text{Na}(2)$

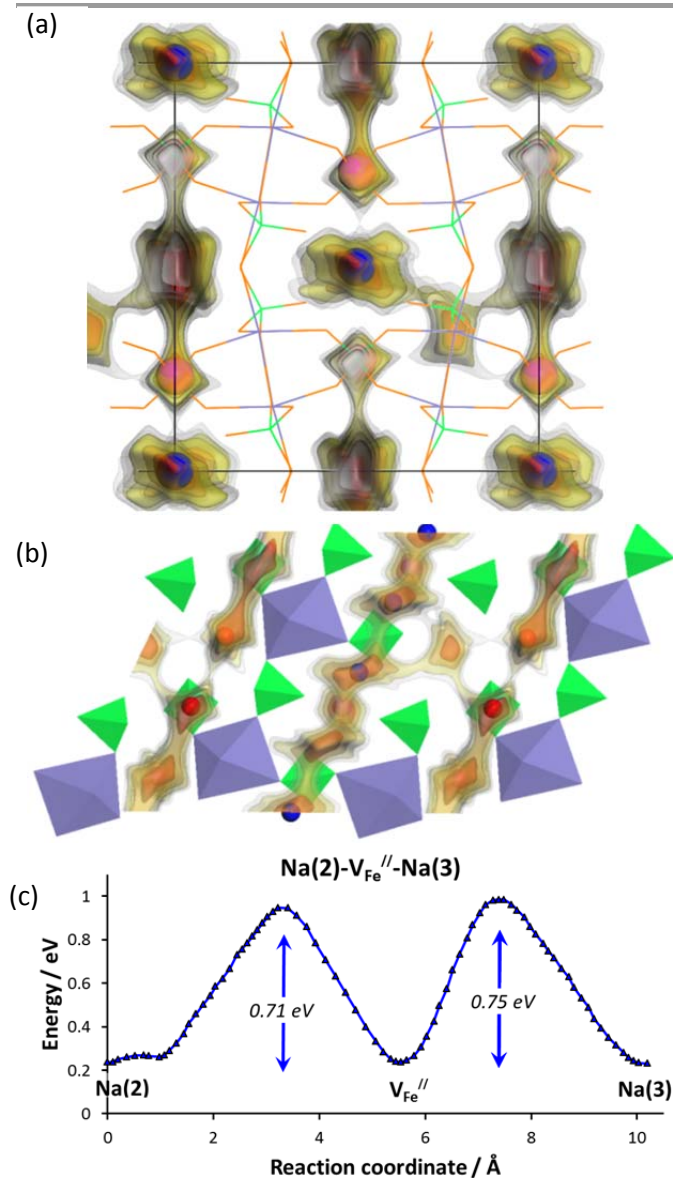


Fig. 4: (a) Isosurfaces of constant BVSE for Na superimposed on the geometry-optimised local structure model of $\text{Na}_{2.25}\text{Fe}_{1.875}(\text{SO}_4)_3$ projected along the c axis. (b) Detail from graph (a) showing a superposition of Na^+ migration pathways for different BVSE values projecting the central portion of the unit cell $0.3 < y < 0.7$ (close to the Fe site vacancy in this local structure model) along the b axis. (c) Migration energy barriers for Na^+ ion diffusion in the same local structure model. Colours of atoms and isosurfaces in (a) and (b) are as for Figure 2.

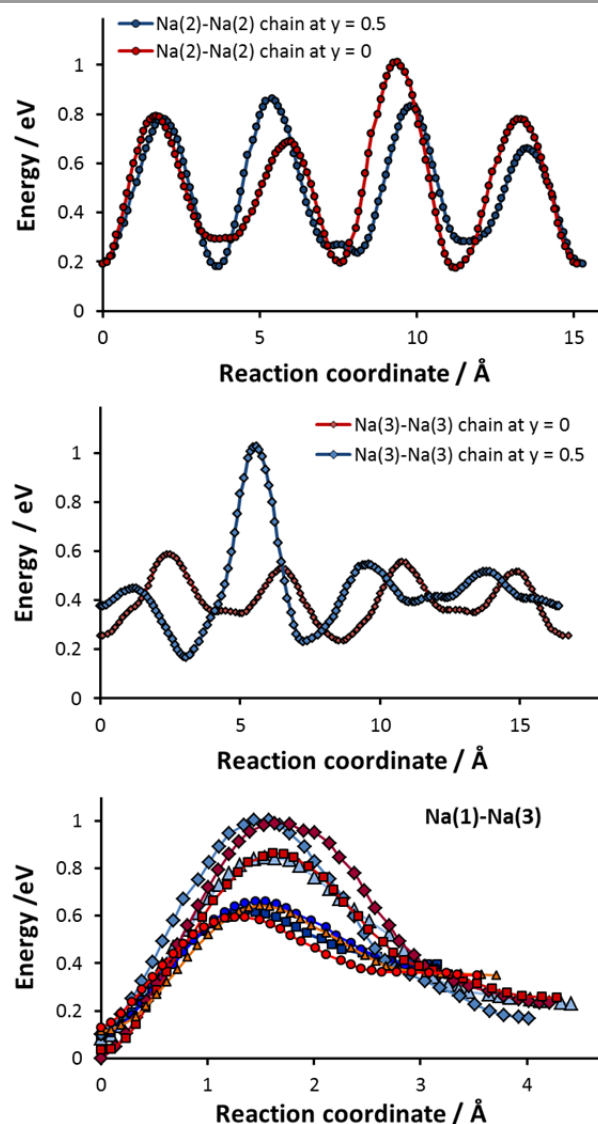


Fig. 5: Migration energy barriers for Na^+ ion diffusion along $\text{Na}(2)$ - $\text{Na}(2)$ chains (top), $\text{Na}(3)$ - $\text{Na}(3)$ chains (center) and for $\text{Na}(1)$ - $\text{Na}(3)$ hops in the geometry-optimized local structure model of $\text{Na}_{2.25}\text{Fe}_{1.875}(\text{SO}_4)_3$ shown in Figure 4. Blue symbols refer to paths at $y \approx 0.5$ in the vicinity of the iron vacancy in this model, while red symbols refer to paths at $y \approx 0.5$ farther away from the built-in defect.

link requires a lower activation energy than the continuation of the path along the Na(3)-Na(3) channel. The spread of local migration barriers along the Na(2)-Na(2) chains 0.62(11) eV appears to be significantly smaller.

The migration barriers between Na(3) and Na(1) observed for the local structure model are on average slightly reduced to 0.7(2) eV, and clearly fall into two equally-sized classes of significantly decreased barriers 0.52(4) eV and 0.87(10) eV (cf. Figure 5) depending on relaxations in response to the site occupancy and local sodium distribution.

3.3. DFT calculations

To achieve a more straightforward comparison between bond valence site energy based calculations and ab initio data for the same chemical composition, we complemented the BVSE analysis by DFT calculations for analogous local structure models derived from a $1 \times 1 \times 2$ supercell of the experimental average structure. Consistent to the model employed in our BVSE calculations (see section 3.2) and the experimentally observed occupancies, the Na(1) site in the initially constructed $\text{Na}_{18}\text{Fe}_{15}\text{S}_{24}\text{O}_{96}$ model assumes that is fully occupied, while randomly 75% of the Na(2) sites, 50% of the Na(3) sites and 15 out of 16 Fe sites are occupied. The initial model was then relaxed by DFT geometry optimisation, which did not alter the sodium distribution onto the three site types. Among the site energies (ionic ionisation energies) of the Na atoms in the local structure model, the lowest energy is found for one of the Na(1) and the highest for one of the Na(3). The site energy is strongly influenced by the distance to the iron vacancy site and the difference between the average site energies may not be significant (e.g. the average site energy of the occupied Na(1) is only 0.12 ± 0.12 eV lower than for the occupied Na(2)). Starting from the $P2_1/c$ or $C2/c$ structure models yielded undistinguishable geometry-optimised structure models.

Table 1 compares the formation energy of the equilibrated model (-115.599 eV/formula unit) to the formation energies of related structure models where the distribution of Na on the four types of sites was slightly modified from {8Na(1), 6Na(2), 4Na(3)} to {7Na(1), 7Na(2), 4Na(3)}, {7Na(1), 6Na(2), 5Na(3)}, {8Na(1), 5Na(2), 5Na(3)} or {8Na(1), 7Na(2), 3Na(3)}.

Table 1. Dependence of formation energy of local structure models on the distribution of the 18 Na^+ in the superstructure.

Configuration {Na(1), Na(2), Na(3)}	Calculated energy (eV/formula unit)	Energy difference (eV/cell)
{8, 6, 4}	-115.599	0.000
{7, 7, 4}	-115.428	1.371
{7, 6, 5}	-115.398	1.612
{8, 5, 5}	-115.454	1.163
{8, 7, 3}	-115.383	1.729

While the detailed increases in energy by 1.1 to 1.7 eV/cell of the geometry-optimised models with altered sodium distributions when compared to the equilibrated model may be influenced by the arbitrary choices of the sites with changed occupancy, the calculations overall demonstrate that the

experimentally observed occupancy indeed constitutes the global minimum.

For the symmetric elementary migration steps Na(3)-Na(3) and Na(2)-Na(2) along the two separate parallel sodium migration channels we estimated migration barriers in a simplified way. To this end we compared the energies of the equilibrated configuration to the energy of a transition state, where the respective mobile sodium is fixed at the centre between two equivalent Na(i) sites. We again found that the lowest migration energy of 0.308 eV is required for Na(3)-Na(3) hops, while for the elementary migration step within the Na(2) channel an activation energy of 0.771 eV was noted. Both values are within the range observed for the empirical treatment of an analogous local structure model (cf. section 3.2.). Compared to the literature ab initio study of $\text{Na}_{0.125}\text{Fe}_2(\text{SO}_4)_3$ it appears that the higher sodium content leads to somewhat higher energy barriers, but does not cause a fundamental change of the ratio of different energy barrier heights.

As to be expected, the concentration of sodium in the structure is closely related to the charges carried by iron atoms. Examination of charges using Bader's analysis³¹ shows that the average charge carried by each atom type is independent of the site configuration. The Fe closest to the iron vacancy carries the highest positive charge (0.035 e higher than the average charge of the other 14 Fe atoms $1.413 \pm 0.006 e$). When one or two sodium atoms are removed from the structure, charges carried by sodium, sulphur and oxygen vary insignificantly, but the average charge on each iron atom increases by about 0.025 e per removed Na (i.e. by 0.41 e or 0.76 e summed up over all 15 Fe) and the standard deviation of the iron charges increases moderately to 0.016 e for $\text{Na}_{17}\text{Fe}_{15}\text{S}_{24}\text{O}_{96}$ and 0.025 e for $\text{Na}_{17}\text{Fe}_{15}\text{S}_{24}\text{O}_{96}$.

3.4. Molecular dynamics simulations

To gain a deeper understanding how pathways in such local structures affect the temperature dependence and anisotropy of the long range ion mobility, a series of molecular dynamics simulations have been performed in a $2 \times 2 \times 3$ supercell of composition $\text{Na}_{108}\text{Fe}_{90}(\text{SO}_4)_{144}$ using our empirical BVSE-based *softBV* forcefield. Na^+ diffusion constants derived from mean square displacement vs. time plots of simulations extending up to 60 ns at 14 temperatures in the range 300 – 800 K show that at room temperature ionic conductivity is dominated by the one-dimensional migration within the Na(3)-Na(3) channels.

As seen from Figure 6, where the diffusion coefficients observed in our MD simulations are displayed as Na^+ ionic conductivities (assuming validity of the Nernst-Einstein rule), the activation energy up to ca. 450 K is found to be 0.29 eV. This means the diffusion coefficient in this extrinsic regime is dominated by the lowest migration barrier, i.e. the one for the fast-ion conducting Na(3)-Na(3) channels. We also found that there is no significant statistical correlation between subsequent ion hops for the temperature range studied, so that applying the Nernst-Einstein rule appears to be justified. At first sight this

may be surprising given the low-dimensional pathways, but the high fraction of vacant sites (ca. 50%) within the Na(3) chains and the sufficient distance between the Na(3) sites allow for an independent occupancy and hence a high success probability of $\text{Na}(1) \rightarrow \text{V}_{\text{Na}(3)}$ or $\text{Na}(3) \rightarrow \text{V}_{\text{Na}(3)}$ hops. Overall these hops do not significantly alter the hopping probability for neighbouring Na(3). For the “intrinsic” regime at temperatures exceeding 450 K the activation energy increases to 0.67 eV as (i) the number of mobile charge carriers gradually increases by Na(1) entering the Na(3) chains (the time-averaged occupancy of Na(3) sites increased by about 4% from 300 K to 750 K), (ii) Na(2) become mobile within the separate Na(2)-Na(2) chains and (iii) $\text{V}_{\text{Fe}^{II}}$ sites bridging the two types of ion-conducting channels become accessible to mobile Na^+ . The three processes have similar activation energies and in detail their respective contributions will be affected by the local structure, in particular by the distribution of Fe defects.

At all temperatures the conductivity component σ_{\parallel} along the channels in c-direction clearly dominates. In the temperature range 300 K – 450 K the ionic conductivity components perpendicular to the channels are too small to be quantified from our MD simulations. For higher temperatures the transport in the perpendicular directions gradually gains ground, but even at 750 K the ratio $\sigma_{\parallel}:\sigma_{\perp}$ is still about 13:1. Accordingly, in the temperature range 300 K – 450 K the transference number is $t_{\text{Na}(3)} \approx 1$ for the 22% of the atoms that are located on Na(3) sites at the beginning of the respective MD simulations (and $t_{\text{Na}(1)} \approx t_{\text{Na}(2)} \approx 0$ for the 78% of Na on Na(1) and Na(2)). In the high temperature “intrinsic” regime all types of Na^+ significantly contribute to the ionic conductivity. For $T = 750$ K we find transference numbers of $t_{\text{Na}(1)} = 0.16(2)$, $t_{\text{Na}(2)} = 0.11(1)$, $t_{\text{Na}(3)} = 0.73(4)$ averaged over results from two MD simulations. It should be noted that the relatively high contribution from atoms initially on Na(1) sites is essentially due to their enhanced mobility once they hop onto Na(3) channel sites.

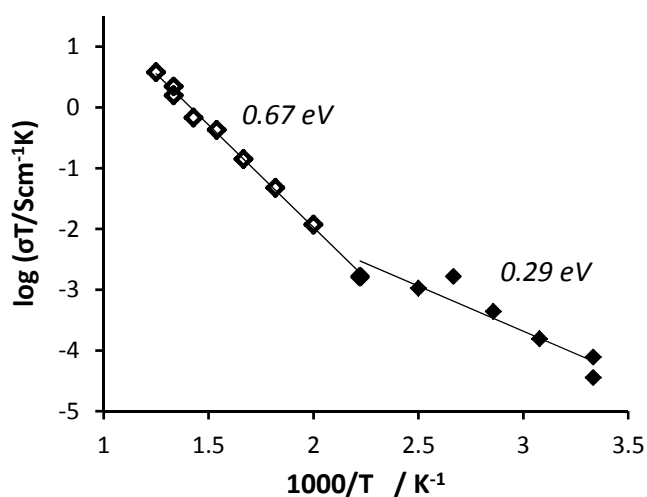


Fig. 6: Arrhenius plot of the temperature dependence of Na-ionic conductivity as derived from molecular dynamics simulations of a $\text{Na}_{2.25}\text{Fe}_{1.875}(\text{SO}_4)_3$ supercell. Conductivities have been derived from the Na^+ ion mobilities assuming validity of the Nernst-Einstein rule.

It may be noted that on the timescale of our NVT simulations Fe^{2+} is found to be immobile except for a single hop of a Fe^{2+} to a Na(3) channel at the highest studied temperature (800 K). While the Fe^{2+} deficiency is highly relevant for the dimensionality of the pathways and the dual role of antisite defects ($\text{Fe}_{\text{Na}(2)}$ or $\text{Fe}_{\text{Na}(3)}$) will block the fast-ion conducting channels, Na_{Fe} will open up additional links between channels)^{23,32} arising from the non-equilibrium low-temperature synthesis routes may have to be factored in, Fe^{2+} mobility can be ruled out as a significant contribution to charge transport in the practically accessible temperature range.

Conclusions

Room temperature ion migration in this alluaudite-type compound is, as suggested in ref. [15], highly anisotropic and almost entirely due to the high Na^+ mobility along the Na(3)-Na(3) channels. The value of the room temperature ionic conductivity $\sigma_{300\text{K}} = 2 \times 10^{-7} \text{ S.cm}^{-1}$ found in our MD simulations clarifies that ion migration is suitably fast to classify the cathode material as promising for adequately high rate performance without a need for nanostructuring. It should, however, be emphasized that the extent of iron deficiency as well as the actual local distribution of the iron vacancies will play a vital role for practical performance: The cross-linking of Na^+ migration pathway across iron vacancies prevents easy blockage of the one-dimensional channels for fast ionic conductivity, but will on the other hand reduce the mobility along the Na(3)-Na(3) channels. Similarly, in $\text{Na}^+/\text{Fe}^{2+}$ antisite defects (whose concentration will due to the non-equilibrium low temperature synthesis routes probably exceed the thermodynamic equilibrium value) the moderately mobile Na_{Fe} will promote transport perpendicular to the chains, but the Fe_{Na} will – in a more drastic way – block ion migration along the chains.

Substituting iron by main group cations to synthesize (electronically insulating) fast-ion conducting solid electrolytes, as suggested in ref. [15], will face the challenge that their conductivity will probably not reach the order of magnitude of other known fast Na^+ -ion conductors. Moreover, the substituting cation (like iron) has to be slightly deficient so that the vacancies can act as links between the otherwise one-dimensional ion migration pathways that would be highly vulnerable to blocking by defects. Likewise using partly desodiated $\text{Na}_{2+\delta-\gamma}\text{Fe}_{2-\delta/2}(\text{SO}_4)_3$ as a lithium intercalation cathode (as explored experimentally for the case of $\text{Na}_{0.89}\text{Fe}_{1.8}(\text{SO}_4)_3$ in ref. [16]), will almost inevitably lead to less favourable rate performance. Li^+ ions will also be mobile preferably along the Na(3)-Na(3) channels, but the lithium migration pathway network will be less robust due to the “mixed-alkali effect”,³³ here the blocking of Li^+ pathway cross-links by Na^+ on Na(1) sites in line with what is observed experimentally.

Acknowledgements

This research was supported by the National Research Foundation, Prime Minister's Office, Singapore under its Competitive Research Programme (CRP Awards NRF-CRP 10-2012-6 and NRF-CRP 8-2011-4). Scholarships to L.L. Wong (jointly funded by NUS and Johnson Matthey PLC) as well as to H.M. Chen (funded by the National Research Foundation, Prime Minister's Office, Singapore) are gratefully acknowledged.

Notes and references

^a Department of Materials Science and Engineering, National University of Singapore, Singapore 117575 (Singapore). E-mail: mseasn@nus.edu.sg.

- 1 V. Palomares, M. Casas-Cabanas, E. Castillo-Martínez, M.H. Han and T. Rojo. *Energy Environ. Sci.* 2013, 6, 2312.
- 2 M.H. Han, E. Gonzalo, G. Singh and T. Rojo, *Energy Environ. Sci.* 2015, 8, 81-102 (doi: 10.1039/C4EE03192J).
- 3 J.F. Whitacre, T. Wiley, S. Shanbhag, Y. Wenzhuo, A. Mohamed, S.E. Chun, E. Weber, D. Blackwood, E. Lynch-Bell, J. Gulakowski, C. Smith and D. Humphreys, *Journal of Power Sources* 2012, 213, 255-264.
- 4 S. Okada, Y. Takahashi, T. Kiyabu, T. Doi, J. Yamaki, T. Nishida, ECS Meeting Abstract 2006, 201, MA2006-02.
- 5 N. Yabuuchi and S. Komaba. *Sci. Technol. Adv. Mater.* 2014, 15, 043501.
- 6 N. Yabuuchi, M. Kajiyama, J. Iwatate, H. Nishikawa, S. Hitomi, R. Okuyama, R. Usui, Y. Yamada and S. Komaba, *Nat. Mater.* 2012, 11, 512-517.
- 7 A.K. Padhi, K.S. Nanjundaswamy and J.B. Goodenough, *J. Electrochem. Soc.* 1997, 144, 1188-1194.
- 8 P. Moreau, D. Guyomard, J. Gaubicher and F. Boucher, *Chem. Mater.* 2010, 22, 4126-4128.
- 9 B.L. Ellis, W.R.M. Makahnouk, Y. Makimura, K. Toghill, and L.F. Nazar, *Nat. Mater.* 2007, 6, 749-753; B.L. Ellis, L.F. Nazar, *Curr. Opin. Solid State Mater. Sci.*, 2012, 16, 168.
- 10 H. Kim, I. Park, D.-H. Seo, S. Lee, S.-W. Kim, W. J. Kwon, Y.-U. Park, C. S. Kim, S. Jeon and K. Kang, *J. Am. Chem. Soc.* 2012, 134, 10369-10372.
- 11 P. Barpanda, Tian Ye, S.-i. Nishimura, S.-C. Chung, Y. Yamada, M. Okubo, H. Zhou and A. Yamada, *Electrochem. Commun.* 24 (2012) 116-119.
- 12 P. Barpanda, M. Ati, B.C. Melot, G. Rousse, J.-N. Chotard, M.-L. Doublet, M.T. Sougrati, S.A. Corr, J.-C. Jumas and J.-M. Tarascon, *Nat. Mater.* 2011, 10, 772-779.
- 13 P. Barpanda, J.-N. Chotard, N. Recham, C. Delacourt, M. Ati, L. Dupont, M. Armand and J.-M. Tarascon, *Inorg. Chem.* 2010, 49, 7401-7413.
- 14 M. Ati, L. Dupont, N. Recham, J.N. Chotard, W.T. Walker, C. Davoisne, P. Barpanda, V. Sarou-Kanian, M. Armand and J.M. Tarascon, *Chem. Mater.* 2010, 22, 4062-4068.
- 15 P. Barpanda, G. Oyama, S.-i. Nishimura, S.-C. Chung and A. Yamada. *Nat. Comm.* 2014, 5, 4358 (doi:10.1038/ncomms5358).
- 16 J. Ming, P. Barpanda, S.-i. Nishimura, M. Okubo and A. Yamada. *Electrochem. Commun.* 51 (2015) 19-22. (doi:10.1016/j.elecom.2014.11.009)
- 17 S. Adams and R. Prasada Rao, "Understanding Ionic Conduction and Energy Storage Materials with Bond-Valence-Based Methods" in "Bond Valences" (I.D. Brown, K.R. Poeppelmeier eds.), Springer Berlin Heidelberg, Structure and Bonding 2014, 158, 129-159. (doi:10.1007/430_2013_137)
- 18 S. Adams, *J. Solid State Electrochemistry* 2010, 14, 1787-1792.
- 19 S. Adams and R. Prasada Rao, *J. Mater. Chem.* 2012, 22, 7687-7691.
- 20 S. Adams and R. Prasada Rao, *J. Mater. Chem.* 2012, 22, 1426-1434.
- 21 S. Adams and R. Prasada Rao, *Phys Chem Chem Phys* 2009, 11, 3210-3216.
- 22 S. Adams, "Practical Considerations in Determining Bond Valence Parameters", in "Bond Valences" (I.D. Brown, K.R. Poeppelmeier eds.), Springer Berlin Heidelberg, Structure and Bonding 2014, 158, 91-128. (doi:10.1007/430_2013_96)
- 23 S. Adams and R. Prasada Rao. *Solid State Ionics* 2011, 184, 57-61.
- 24 L.L. Wong, H.M. Chen and S. Adams, in preparation.
- 25 M.J.S. Dewar, E.F. Healy and J.J.P. Stewart, *J. Chem. Soc., Faraday Trans.* 1984, 280, 227.
- 26 J.D. Gale, *J. Chem. Soc. Faraday Trans.* 1997, 93, 629-637.
- 27 Materials Studio 6.0. Accelrys Inc., San Diego, CA 92121-3752, 2012.
- 28 G. Kresse and J. Furthmüller, *Comput. Mater. Sci.* 1996, 6, 15-50.
- 29 P.E. Blöchl, *Phys. Rev. B* 1994, 50, 17953.
- 30 J.P. Perdew, K. Burke and M. Ernzerhof, *Phys. Rev. Lett.* 1996, 77, 3865-3869.
- 31 W. Tang, E. Sanville and G. Henkelman, *J. Phys.: Condens. Matter* 2009, 21, 084204.
- 32 S. Adams, *Applied Energy* 2012, 90, 323-328.
- 33 J. Swenson and S. Adams, *Phys. Rev. Lett.* 2003, 90, 155507.